Materials Advances

ROYAL SOCIETY OF CHEMISTRY

COMMUNICATION

View Article Online
View Journal | View Issue

Cite this: *Mater. Adv.*, 2025, 6, 3058

Received 17th December 2024,
Accepted 23rd March 2025

DOI: 10.1039/d4ma01253d

rsc.li/materials-advances

Efficient self-powered near-infrared organic photodetectors with a self-assembled transport layer†

Jiazhen Cao,[a] Xing Guo,[b] Haimei Wu,[c] Jingjing Chang [b] and Qingzhen Bian [*a]

An efficient self-powered organic photodetector with a self-assembled 4PACz material as the hole transport layer was prepared, and the device demonstrates long-term stability with a responsivity of 0.4 A W^{-1}, fast response time of 7.2 μs and specific detectivity of over 10^{12} Jones in the near-infrared range.

Introduction

Organic photodetectors (OPD) are devices that convert optical signals into electrical signals, and have been applied in many fields, including artificial intelligence, medicine, defense, imaging, communication, *etc.*[1–6] The improvement of OPD device performance is related to the development of materials and device structures. Among the materials candidates for high-efficiency devices, A–D–A-structured small molecules are extremely promising as they exhibit superior energy level tunability, and good molecular crystallinity. The multiple D–A interactions increase the backbone interaction between the adjacent acceptor molecules and/or the polymer donor in the blend film, facilitating molecular aggregation and electron transport, while also contributing to phase aggregation.[7] Organic photodetectors with bulk heterojunction structures have a similar device structure to organic photovoltaic devices[8] and phototransistors,[9] and the uniform distribution of donors (D) and acceptors (A) in the active layer demonstrates serious phase separation, and is detrimental to the long-term stability of the device.[10] To solve the phase separation issue, researchers have tried different methods, including adjusting the donor acceptor ratios, using different solvent solutions, using thermal or solvent annealed films, *etc.*[11–14]

The introduction of a transport layer further improves the charge injection/transport process at the electrode interfaces, and normally results in enhancement of the organic photodetector performance. However, the traditional hole transport layer (HTL) material PEDOT:PSS (poly(3,4-ethylenedioxythiophene) polystyrene sulfonate) is water-soluble and susceptible to water vapor, and is detrimental to the stability of the device.[15] In recent years, self-assembled materials have been used as the hole transport layer in photovoltaic devices, due to their adjustable energy levels, low cost, high light transmittance, and passivation with transparent conductive oxide substrates.[16–20] Some self-assembled monolayers exhibit limited dipole orientation on indium tin oxide (ITO),[21–24] and flexible devices based on self-assembled films are also highly durable.[25,26] By changing the end groups, the self-assembled transport material can also be further modified to improve the device performance.[27–30]

In this work, to improve the device performance and long-term operational stability, an efficient near-infrared organic photodetector with a diluted D/A ratio of 1 : 19 based on the PM6:L8-BO structure was successfully prepared. The traditional balanced D/A ratio in the active layer induced serious phase separation, while the diluted D/A ratio results in high donor or acceptor phase purity, which benefits the long-term operational stability of the device. Furthermore, one self-assembling hole transport layer 4PACz ((4-(9*H*-carbazol-9-yl)butyl)phosphonic acid) was introduced, to replace the traditional PEDOT:PSS material, and an efficient organic photodetector with long-term operational stability was obtained. The resulting photodetector exhibited a peak responsivity close to 0.4 A W^{-1} at 800 nm and resulted in a specific detectivity of over 5 × 10^{12} Jones at near-IR (NIR) wavelengths, and a fast response time of 7.2 μs. The corresponding flexible device based on the PET/ITO substrate with an additional 30% polystyrene (PS) in the 4PACz layer was also prepared, further improving the flexibility and detection performance, with a maximum responsivity of close to 0.28 A W^{-1} and specific detectivity of over 10^{11} Jones.

[a] *Laboratory of Advanced Quantum Bio-optoelectronics (LAQB), Xi'an Modern Chemistry Research Institute, Xi'an, 710065, China. E-mail: qinbi65@hotmail.com*
[b] *Advanced Interdisciplinary Research Center for Flexible Electronics, Academy of Advanced Interdisciplinary Research, Xidian University, Xi'an 710071, China*
[c] *Xi'an Key Laboratory of Liquid Crystal and Organic Photovoltaic Materials, State Key Laboratory of Fluorine and Nitrogen Chemicals, Xi'an Modern Chemistry Research Institute, Xi'an, 710065, China*

† Electronic supplementary information (ESI) available. See DOI: https://doi.org/10.1039/d4ma01253d

Results and discussion

Here, the polymer PM6 (poly[(2,6-(4,8-bis(5-(2-ethylhexyl-3-fluoro)-thiophen-2-yl)-benzo [1,2-*b*:4,5-*b*′]dithiophene))-*alt*-(5,5-(1′,3′-di-2-thienyl-5′,7′-bis(2-ethylhexyl)-benzo [1′,2′-*c*:4′,5′-*c*′]dithiophene-4,8-dione))]) and small molecular L8-BO (2-[2-[[8,22-bis(2-butyloctyl)-23-[[1-(dicyanomethylidene)-5,6-difluoro-3-oxoinden-2-ylidene]methyl]-3,27-bis(2-ethylhexyl)-6,10,15,20,24-pentathia-3,14,16,27-tetrazaoctacyclo[16.9.0.02,12.04,11.05,9.013,17.019,26.021,25]heptacosa-1(18),2(12),4(11),5(9),7,13,16,19(26),21(25),22-decaen-7-yl]methylidene]-5,6-difluoro-3-oxoinden-1-ylidene]propanedinitrile) were introduced as donor and acceptor, respectively. The transport materials are PEDOT:PSS and 4PACz, respectively, and photodetectors with different D/A ratios from 1 : 1.2 to 1 : 19 were prepared. The structure diagram of the device and energy levels, chemical structures of related materials and absorption are shown in Fig. 1. The OPDs are prepared with a structure of ITO/PEDOT:PSS/PM6:L8-BO/PDINO/Al and ITO/4PACz/PM6:L8-BO/PDINO/Al. The current–voltage curves and external quantum efficiency (EQE) characterization of the devices are shown in Fig. 2 and Fig. S1–S4 (ESI†). For PEDOT:PSS based devices, compared to optimized devices (with D/A ratios of 1 : 1.2), the diluted devices (with D/A ratios of 1 : 19) demonstrated a significantly decreased EQE and photocurrent value (Fig. S4, ESI†). Due to reduced non-radiative recombination loss,[31] the open circuit voltage is significantly improved in the diluted 1 : 19 blend (Fig. S1, ESI†). As a comparison, for the 4PACz based devices, the photocurrent of the diluted devices is slightly decreased compared to the device with a normal D/A ratio (1 : 1.2) (Fig. 2a). The light detection performance was also improved after the self-assembled transport layer 4PACz was introduced. Specifically, the EQE value in the range of 650–850 nm is slightly increased from 83% (PEDOT:PSS material) to 91% (4PACz material) for the optimized devices, while it is significantly increased from the original 40% (PEDOT:PSS material) to 60% (4PACz material) for the diluted (1 : 19) devices (Fig. 2(b) and (c)). To the best of our knowledge, the value of 91% is among the highest EQE values of organic photodetector devices. These results suggest that the self-assembled 4PACz benefits interfacial charge transport between the electrode and active layer, and results in a higher photocurrent and EQE value (Fig. 2b and c) in the diluted PM6:L8-BO blends, compared to the PEDOT:PSS based devices. It is noted that the photocurrent was found to increase linearly with irradiance up to $\sim 10^{-1}$ W cm^{-2}, *i.e.*, over five orders of magnitude both in diluted (1 : 19) and optimized (1 : 1.2) devices (Fig. S3, ESI†), and comparable linear dynamic ranges (LDR) ($\sim$110 dB) can be obtained at 0 V.

The device operational stability is critical for future commercial applications, and to explore long-term device performance, all of the above devices were stored in air for 50 days. The device with a PEDOT:PSS interfacial layer was completely non-functional after 50 days in air, and as a comparison, the detectivity performance of the device with a 4PACz interfacial layer was greatly preserved (Fig. 2d). Specifically, the EQE value significantly decreased from 90% to 40% in the range of 700–850 nm for the balanced devices (1 : 1.2), while the EQE value was slightly decreased from 63% to 50% in the

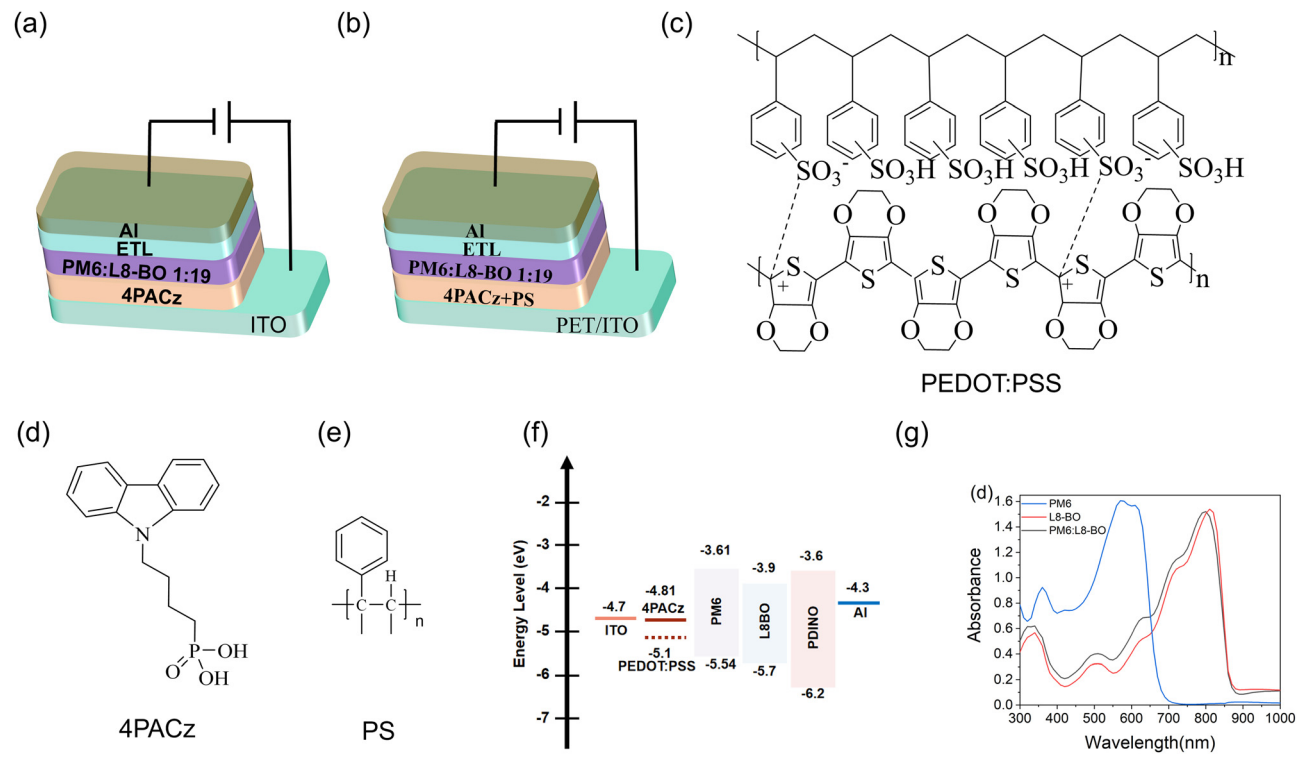

Fig. 1 (a) The rigid ITO and (b) flexible PET/ITO device structures with diluted donor and acceptor ratios. The chemical structures of (c) PEDOT:PSS, (d) 4PACz, and (e) PS. (f) Energy levels of the materials. (g) Absorption spectra of PM6, L8-BO, and diluted PM6:L8-BO blends (1 : 19).

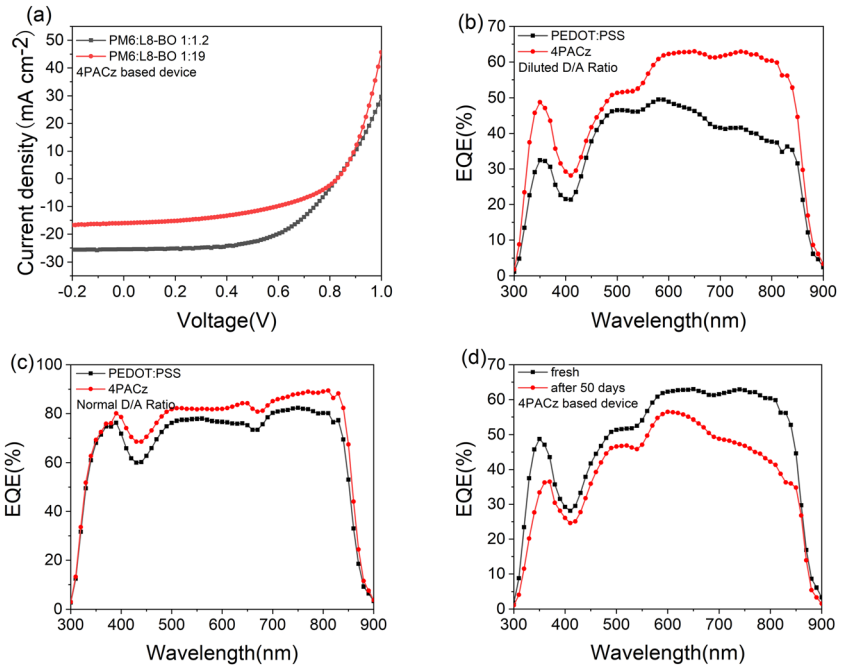

Fig. 2 (a) *J*–*V* curves of devices with normal D/A ratios and diluted D/A ratios. (b) EQE comparison of diluted organic photodetectors with different interfacial layers. (c) EQE comparison of 4PACz and PEDOT:PSS based organic photodetectors. (d) EQE of the diluted device with 4PACz as the HTL layer after 50 days in air.

range of 700–850 nm for the diluted devices (1 : 19). Previous studies indicate that the monolayer interfacial materials benefit interfacial charge transport with interfacial dipole contributions, and this results in an improvement in the photovoltaic device stability.[20–25] Furthermore, compared to the balanced devices (1 : 1.2), the diluted devices (1 : 19) exhibit greater D/A domain purity, which also contributes to the improvement of the device stability. These results suggest that the self-assembled transport layer 4PACz can indeed improve the long-term stability of the PM6:L8-BO device performance, especially for diluted devices (Fig. S4, ESI†).

To further characterize the performance of the prepared organic photodetectors, the responsivity (R) and specific detectivity (D^*) of the devices are calculated (see the ESI†). The results are shown in Fig. 3(a) and (b). Compared to the PEDOT:PSS based device, both responsivity and detectivity are significantly improved in the 4PACz based devices, as 4PACz demonstrates a suitable energy level, better transmittance and interfacial dipole contribution. The device performance is summarized in Table S1 (ESI†). Specifically, the responsivity around 800 nm is close to 0.4 A W^{-1} for the 4PACz based diluted device, which is among the highest values in organic photodetectors at NIR wavelengths, and the related D^* is in the order of magnitude of 10^{12} Jones. The repeatabilities of the fabricated OPDs were further investigated. The distribution of the EQE values is illustrated in Fig. S6 (ESI†), and the corresponding R and D^* are illustrated in Fig. S7 and S8 (ESI†), respectively. According to the Gaussian function fitting result (shown as red curves), the average R values of the fabricated normal OPDs and diluted OPDs (based on the 4PACz layer) are around 0.50 A W^{-1} and 0.35 A W^{-1}, respectively. The corresponding D^* values are around 7.0×10^{12} Jones and 4.7×10^{12} Jones, and approximately 80% of the D^* values of the devices are located near the average value, indicating that the fabricated devices demonstrated excellent device reproducibility. The response speed is another significant parameter of OPDs, which is very important for optical communication and imaging applications. We also measured the time-dependent response of the photodetector. Fig. 3(c) shows the photocurrent response of the device at no applied bias. From the diluted photodetector responses, fall times, t_f (time for the photoresponse to decrease from 90 to 10%), of 4.5 μs for the PEDOT:PSS based device and 7.2 μs for the 4PACz based device were obtained, respectively. Such response speed values are among the best for organic or perovskite photodetectors measured at no external bias.

For future commercial organic photodetector applications, good mechanical flexibility and stretching ability need to be further considered.[32–34] To further explore the self-assembled transport layer in diluted PM6:L8-BO organic photodetectors, a small amount of polystyrene (30%) was introduced into the 4PACz layer, and the corresponding flexible device was obtained (Fig. 1(b)). The current–voltage characterization and device parameters are summarized in Fig. S9 and Tables S1–S3 (ESI†). The responsivity and detectivity behaviours of the diluted organic photodetector devices are shown in Fig. 4a and Fig. S10 (ESI†). Compared to the 4PACz based flexible device, the device performance in the range of 600–650 nm is slightly improved from 0.26 A W^{-1} to 0.29 A W^{-1} after inserting polystyrene (PS), and such a value is comparable to the performance of an ITO glass based device. Furthermore, the long-term stability of flexible devices also demonstrates similar features to ITO glass based devices, even after several stretching/bending cycles. Specifically, the EQE value was slightly decreased from 65% to 45% in the range of 700–850 nm for diluted devices (1 : 19). After introducing

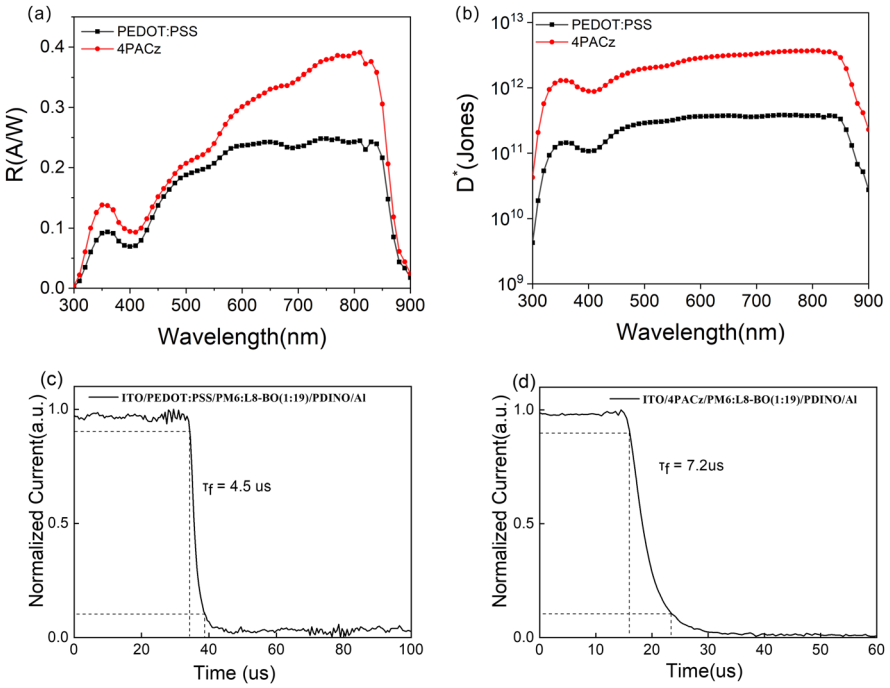

Fig. 3 (a) Responsivity results in diluted organic photodetector devices. (b) Detectivity results in diluted organic photodetector devices. (c) Response speed of PEDOT:PSS based organic photodetector devices. (d) Response speed of 4PACz based organic photodetector devices.

PS to 4PACz blends, the long-term device performance became even better, the EQE value slightly decreased from 60% to 48%, and the corresponding responsivity value decreased from 0.37 A W^{-1} to 0.27 A W^{-1} (Fig. S11, ESI†). The surface morphologies of the HTL layer (with and without PS) with the active layer were studied in detail by atomic force microscopy (AFM) (Fig. 4 and Fig. S13, ESI†). After blending PS in the 4PACz, the resulting film exhibits an increased roughness value (increased from 2.8 nm to 7.9 nm) and nanofibril features. Previous studies demonstrate that the interfacial nanofibril features result in nanocontact at the electrode and efficient charge extraction can be obtained in flexible organic heterojunction diodes.[35] Furthermore, PS appears

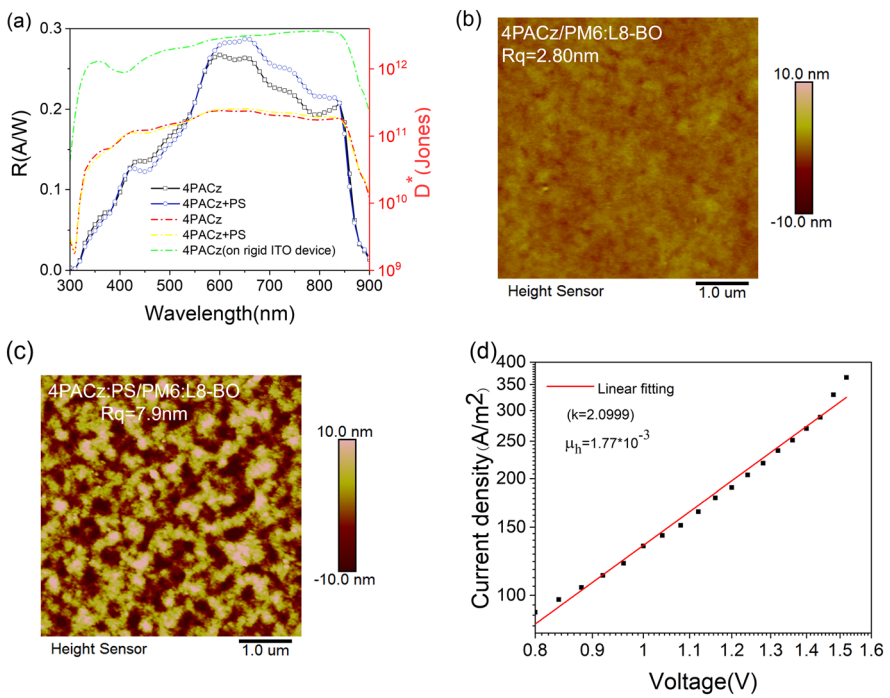

Fig. 4 (a) Responsivity and detectivity of flexible diluted organic photodetector devices. (b) AFM height image of 4PACz based films. (c) AFM height image of 4PACz:PS based films. (d) SCLC of the diluted device after introducing PS in the 4PACz HTL layer.

frequently to work as the intermediate layer for modulating interfacial charge transfer.[36–38] Thus, inserting PS in the 4PACz layer in flexible devices results in a high roughness value and nanofibril features, forming a nanocontact with the electrode, and further improving charge extraction at the electrode with high mechanical flexibility. This conclusion can also be further confirmed by the hole mobility value, as the hole transport mobility was significantly increased from 2.79×10^{-7} cm^2 V^{-1} s^{-1} (Fig. S10a, ESI†) to 1.77×10^{-3} cm^2 V^{-1} s^{-1} (Fig. 4d) after inserting PS.

Conclusions

We have successfully prepared a series of efficient PM6:L8-BO organic photodetectors with an unbalanced D/A ratio, and further improved the photodetector performance with one self-assembled 4PACz transport layer. In contrast to previous reports on bulk heterojunctions, we demonstrated that diluted blends with an unbalanced D/A ratio exhibit high photodetector performance and long-term device stability. We also show that such photodetectors exhibit a response time of 7.2 μs, and the specific detectivity reaches 5×10^{12} Jones at NIR wavelengths without external bias. Finally, compared to bulk heterojunctions with balanced D/A ratios, the diluted organic photodetector exhibits an improvement in the long-term stability in air, whether on glass substrates or flexible PET substrates. We thus believe that the present work re-opens the door to exploring the dilution strategy and monolayer interfacial materials for organic photodetectors that can exploit the unique strategy of combining long-term device stability with high detector performance.

Author contributions

Q. B. designed the whole project; J. C. performed all device-based experiments; X. G. performed the transient photocurrent experiments; J. C. and Q. B. analyzed the data and wrote the draft; all authors discussed the experimental results and commented on the manuscript.

Data availability

The data supporting this article have been included as part of the ESI.†

Conflicts of interest

There are no conflicts to declare.

Acknowledgements

This work has been supported by the financial support from National Natural Science Foundation of China (Grant 62205268).

Notes and references

1 Y. Wang, T. Zhang and D. Samigullina, *Adv. Funct. Mater.*, 2024, **34**, 1.
2 Y. Wang, J. Kublitski and S. Xing, *Mater. Horiz.*, 2022, **9**, 220–251.
3 H. Ren, J. D. Chen and Y. Q. Li, *Adv. Sci.*, 2021, **8**, 2002418.
4 J. Liu, Y. X. Wang and H. Wen, *Sol. RRL*, 2020, **4**, 2000139.
5 Z. Lv, S. Yan and W. Mu, *Adv. Mater. Interfaces*, 2023, **10**, 2202130.
6 D. Yang and D. Ma, *Adv. Opt. Mater.*, 2019, **7**, 1800522.
7 J. Yuan, H. Zhang and R. Zhang, *Chemistry*, 2020, **6**, 2147–2161.
8 A. Wadsworth, Z. Hamid and J. Kosco, *Adv. Mater.*, 2020, **32**, 2001763.
9 Y. Lu, L. Liu and R. Gao, *Light-Sci. Appl.*, 2024, **13**, 318.
10 L. Zhao, H. Wang and H. Ji, *APL Mater.*, 2023, **11**, 120601.
11 X. Zhao, M. Liu and J. Wang, *ACS. Appl. Mater. Interfaces*, 2024, **16**, 35400–35409.
12 K. W. Tsai, G. Madhaiyan and L. H. Lai, *ACS. Appl. Mater. Interfaces*, 2022, **14**, 38004–38012.
13 J. Qin, Z. Chen and P. Bi, *Energy Environ. Sci.*, 2021, **14**, 5903–5910.
14 X. Si, Y. Huang and W. Shi, *Adv. Funct. Mater.*, 2023, **33**, 2306471.
15 Q. Kang, Z. Zheng and Y. Zu, *Joule*, 2021, **5**, 646–658.
16 M. Li, M. Liu and F. Qi, *Chem. Rev.*, 2024, **124**, 2138–2204.
17 S. Casalini, C. A. Bortolotti and F. Leonardi, *Chem. Soc. Rev.*, 2017, **46**, 40–71.
18 Y. Li, Z. Jia and P. Huang, *Adv. Energy Mater.*, 2024, **14**, 2304000.
19 P. Gao, C. Li and Y. Chen, *Energy Environ. Sci.*, 2024, **17**, 6157–6203.
20 I. G. Sonsona, M. Carrera and M. Más-Montoya, *ACS Appl. Mater. Interfaces*, 2023, **15**, 22310–22319.
21 H. Bin, K. Datta and J. Wang, *ACS Appl. Mater. Interfaces*, 2022, **14**, 16497–16504.
22 A. Al-Ashouri, E. Köhnen and B. Li, *Science*, 2020, **370**, 1300–1309.
23 J. Y. Lin, F. C. Hsu and J. Chang CY, *Mater. Chem. C*, 2021, **9**, 5190–5197.
24 X. Yang, Y. Li and J. Liu, *Nano Lett.*, 2024, **24**, 9385–9390.
25 R. Zhang, Z. Huang and W. Chen, *Adv. Funct. Mater.*, 2023, **33**, 2210063.
26 T. Amrillah, Y. Bitla and K. Shin, *ACS Nano*, 2017, **11**, 6122–6130.
27 A. C. Chang, Y. S. Wu and W. C. Chen, *Adv. Opt. Mater.*, 2024, **12**, 2301789.
28 G. Qu, S. Cai and Y. Qiao, *Joule*, 2024, **8**, 2123–2134.
29 F. H. Isikgor, S. Zhumagali and L. V. T. Merino, *Nat. Rev. Mater.*, 2023, **8**, 89–108.
30 M. Li, Y. Xie and F. R. Lin, *Innovation*, 2022, **4**, 100369.
31 N. Yao, J. Wang and Z. Chen, *J. Phys. Chem. Lett.*, 2021, **12**, 5039–5044.
32 G. Dastgeer, Z. M. Shahzad and H. Chae, *Adv. Funct. Mater.*, 2022, **32**, 2204781.
33 G. Simone, M. J. Dyson and S. C. Meskers, *Adv. Funct. Mater.*, 2020, **30**, 1904205.
34 L. Zhang, N. Pasthukova and Y. Yao, *Adv. Mater.*, 2018, **30**, 1801181.
35 Q. Z. Bian, C. Musumeci and C. F. Wang, *Sci. Bull.*, 2021, **66**, 875–879.
36 A. Lorente, P. Pingel and A. Miasojedovas, *ACS Appl. Mater. Interfaces*, 2017, **9**, 24043–24051.
37 Y. Hou, L. Wang and R. Sun, *ACS Nano*, 2022, **16**, 8358–8369.
38 M. Li, X. Yan and Z. Kang, *ACS Appl. Mater. Interfaces*, 2018, **10**, 18787–18795.